JVI Journals.ASM.org

Molecular Determinants Defining the Triggering Range of Prefusion F Complexes of Canine Distemper Virus

Mislay Avila,[a,b] Lisa Alves,[a,b] Mojtaba Khosravi,[a,b] Nadine Ader-Ebert,[a,b] Francesco Origgi,[c] Jürgen Schneider-Schaulies,[d] Andreas Zurbriggen,[a] Richard K. Plemper,[e,f] Philippe Plattet[a]

Division of Neurological Sciences, DCR-VPH, Vetsuisse Faculty, University of Bern, Bern, Switzerland[a]; Graduate School for Cellular and Biomedical Sciences, University of Bern, Bern, Switzerland[b]; Centre for Fish and Wildlife Health (FIWI), Vetsuisse Faculty, University of Bern, Bern, Switzerland[c]; Institute for Virology and Immunobiology, University of Würzburg, Würzburg, Germany[d]; Center for Inflammation, Immunity and Infection, Georgia State University, Atlanta, Georgia, USA[e]; Department of Pediatrics, Emory University School of Medicine, Atlanta, Georgia, USA[f]

ABSTRACT

The morbillivirus cell entry machinery consists of a fusion (F) protein trimer that refolds to mediate membrane fusion following receptor-induced conformational changes in its binding partner, the tetrameric attachment (H) protein. To identify molecular determinants that control F refolding, we generated F chimeras between measles virus (MeV) and canine distemper virus (CDV). We located a central pocket in the globular head domain of CDV F that regulates the stability of the metastable, prefusion conformational state of the F trimer. Most mutations introduced into this "pocket" appeared to mediate a destabilizing effect, a phenotype associated with enhanced membrane fusion activity. Strikingly, under specific triggering conditions (i.e., variation of receptor type and H protein origin), some F mutants also exhibited resistance to a potent morbillivirus entry inhibitor, which is known to block F triggering by enhancing the stability of prefusion F trimers. Our data reveal that the molecular nature of the F stimulus and the intrinsic stability of metastable prefusion F both regulate the efficiency of F refolding and escape from small-molecule refolding blockers.

IMPORTANCE

With the aim to better characterize the thermodynamic basis of morbillivirus membrane fusion for cell entry and spread, we report here that the activation energy barrier of prefusion F trimers together with the molecular nature of the triggering "stimulus" (attachment protein and receptor types) define a "triggering range," which governs the initiation of the membrane fusion process. A central "pocket" microdomain in the globular F head contributes substantially to the regulation of the conformational stability of the prefusion complexes. The triggering range also defines the mechanism of viral escape from entry inhibitors and describes how the cellular environment can affect membrane fusion efficiency.

Morbilliviruses belong to the *Paramyxoviridae* family and consist of enveloped, single-stranded RNA viruses with negative genome polarity. Among the morbilliviruses, the human pathogen measles virus (MeV) is still responsible for over 120,000 fatalities annually (1), whereas canine distemper virus (CDV) causes high mortality and morbidity not only in dogs but also in an ever increasing spectrum of wild aquatic and terrestrial carnivores (2–4).

To initiate disease, morbilliviruses' infection of target cells is mediated by two envelope glycoproteins: the tetrameric H protein and the trimeric F protein (5). It is thought that H binding to a specific receptor on target cells triggers oligomeric conformational changes of the H stalk domain, which may, in turn, translate into F activation (5–11). As a consequence, prefusion F trimers undergo a series of conformational changes, which are associated with plasma membrane fusion activity, fusion pore formation, and cell entry (5, 12, 13).

H tetramers consist of a short cytosolic tail, a single transmembrane-spanning domain, and a large ectodomain. The ectodomains contain a membrane proximal stalk domain that supports the membrane-distal cuboidal head region (10, 14). X-ray structures of many paramyxovirus attachment protein head domains invariably revealed a six-bladed beta-propeller structure, which serves as the receptor docking region (6, 10, 15–20). Partial crystal structures of the Newcastle disease virus (NDV) and parainfluenza virus type 5 (PIV5) attachment protein (HN) stalks highlighted a common four-helical-bundle (4HB) conformation (21, 22). Many studies documented that the paramyxovirus attachment protein stalk domain physically interacts with F trimers (23–29). H stalks are thought to form short-range contacts with the large globular head domain of trimeric F, which inferred a staggered H-F association model in which H heads would be positioned above F heads (29, 30). This model is substantiated by the finding that truncated, stabilized MeV H stalks lacking the head domains are sufficient to specifically trigger MeV F (31). Several residues and/or microdomains in the F head domains are suggested to participate in H binding (29, 32–35).

The F protein is initially synthesized as a long inactive precursor (F_0) that is matured in the Golgi apparatus into two disulfide-linked subunits (F_1 plus F_2). Like other class I viral fusion proteins, all morbillivirus F monomers contain two highly conserved heptad repeat regions, A and B (HRA and HRB, respectively), a hy-

Received 24 October 2013 **Accepted** 19 December 2013
Published ahead of print 26 December 2013
Editor: D. S. Lyles
Address correspondence to Philippe Plattet, philippe.plattet@vetsuisse.unibe.ch.

doi:10.1128/JVI.03123-13

drophobic fusion peptide (FP), which is located at the N-terminal part of HRA, a single transmembrane-spanning domain located at the C terminus of HRB, and a cytosolic tail (5). An X-ray structure of the PIV5 F trimer in its prefusion form revealed a short three-helical-bundle (3HB) domain formed by HRB that supports a large globular head domain (36). Upon H-dependent F activation, F trimers undergo a series of conformational changes that ultimately result in the generation of a six-helical-bundle (6HB) fusion core, as is typical for class I viral fusion proteins (12). Concerning the nature of the conformational intermediates, it was proposed that (i) the 3HB F-stalk domain dissociates, (ii) the packed HRA segments refold into an extended 3HB structure, allowing the FP to embed in the target cell lipid bilayer (forming a prehairpin intermediate), and (iii) the three dissociated HRB domains swing around the base of the globular head and dock into the grooves of the 3HB structure, creating the thermodynamically stable 6HB structure (5, 13, 36).

We recently demonstrated that F complexes contain a sufficiently high inherent energy barrier to maintain the prefusion state in the absence of H (37, 38), confirming that morbillivirus H is not required as a molecular scaffold stabilizing prefusion F. Upon receptor engagement, the ensuing conformational changes in H rather result in the release of F from intracellularly preformed H/F complexes, suggesting that refolding H tetramers actively reduce the activation energy barrier of metastable prefusion F trimers, either by destabilizing prefusion F or stabilizing a high-energy F fusion intermediate conformation. Consistent with this idea, we and others have recently demonstrated that structural rearrangements within the H-stalk domain are strictly required to initiate F conformational changes (38–40). Taken together, these findings imply that the energy level of metastable prefusion F trimers affects F triggering and thus regulates morbillivirus membrane fusion.

With the overarching aim to better characterize the thermodynamic basis of paramyxovirus membrane fusion, we identified a microdomain in F that controls the conformational stability of the prefusion state without significantly affecting physical interactions with H. We found that destabilized F complexes were resistant to a representative of the AS-48 class (41, 42) of the morbillivirus membrane fusion inhibitor *N*-(3-cyanophenyl)-2-phenylacetamide (3g) (43, 44), a molecule previously shown to block MeV entry (42) by increasing the stability of prefusion F trimers to levels that precluded H-mediated F triggering (37). Moreover, resistance to the compound (AS-48) coincided with increased fusion activity (45, 46). We now extend this notion by demonstrating that resistance mutations locating in a "pocket" microdomain within the globular head domain reduce the stability of prefusion F trimers. In addition, our data reveal that the intensity of the F-triggering stimulus by the H tetramers is influenced by the origin of the H protein and the molecular nature of the receptor contacted.

MATERIALS AND METHODS

Cell cultures and viruses. Vero cells, Vero cells engineered to express the canine SLAM receptor (Vero-cSLAM [kindly provided by V. von Messling]), and Vero cells producing canine nectin-4 (Vero-cNectin-4) were grown in Dulbecco's modified Eagle's medium (Gibco, Invitrogen) with 10% fetal calf serum at 37°C in the presence of 5% CO_2. CHO cells (kindly provided by Beat Trueb, University of Bern) were grown in Dulbecco's modified Eagle's medium (Gibco, Invitrogen) with 10% fetal calf serum at 37°C in the presence of 5% CO_2. The MVA-T7 recombinant vaccinia virus that was used for a quantitative cell-cell fusion assay was obtained from B. Moss, NIH, Bethesda, MD.

Generation of lentiviral vector expressing canine nectin-4 and generation of Vero cells constitutively expressing canine nectin-4. The lentivirus vector pRRL has been described elsewhere (47) and was kindly provided by Patrick Salomon, University of Geneva. The canine nectin-4 gene was synthesized in order to bear an additional N-terminal hemagglutinin (HA) tag (Eurofins). Moreover, the gene was designed to be targeted to the secretory pathway through the IgK signal peptide. The construct was subsequently digested with RsrII and cloned into the pRRL-RsrII-cleaved vector (Eurofins). Stocks of lentivirus vectors were subsequently generated in 293T/17 cells as previously described (48). Finally, three reiterative cycles of lentivirus transduction in Vero cells (multiplicity of infection [MOI] of 10) was performed. Expression of canine nectin-4 in Vero cells was controlled by flow cytometry using the anti-HA monoclonal antibody (MAb) 16B12 (Covance).

Site-directed mutagenesis. All single substitutions, as well as the F chimera, were performed in the pCI-CDV F-wt (expressing wild-type F) (derived from the fusion protein of the A75/17 CDV strain, which also bears an additional ectodomain FLAG-tag epitope) and in pCI-MeV F-Edm (derived from the fusion protein of the Edmonston measles virus strain, which also carries an ectodomain FLAG tag epitope) by using the QuikChange Lightning site-directed mutagenesis kit (Agilent). The pCI-CDV H-wt (A75/17) and pCI-MeV H-Edm (Edmonston) plasmids were previously described (39, 49). F-chim1 contains the following substitutions: V447T, V449M, S450P, S452G, A453T, and I545V. F-chim2 contains all mutations of chimera 1 (Chim 1) and S459A. F-chim3 contains all mutations of Chim 1 and 2 and Q469E, I470L, D473S, and S475K. F-chim4 contains all mutations of chim1, 2, and 3 and T485S, M486F, and K489R.

Transfections and luciferase reporter gene content mix assay. Vero, Vero-cSLAM, and Vero-cNectin-4 cells, in 6-well plates at 90% confluence, were cotransfected with 2 μg of the various pCI-CDV F or MeV F constructs and 1 μg of the either pCI-CDV H or MeV H plasmids with 9 μl of Fugene HD (Roche), according to the manufacturer's protocol. In some experiments, phase-contrast pictures were taken 24 h posttransfection with a confocal microscope (Olympus FluoView FV1000).

The quantitative fusion assay was performed as described previously (50, 51). Briefly, Vero (for CDV H) or CHO (for MeV H) cells were cotransfected with the F and H expression plasmids and 0.1 μg of pTM-Luc (kindly provided by Laurent Roux, University of Geneva). In parallel, separate 6-well plates of Vero, Vero-SLAM, or Vero-cNectin-4 cells at 30% confluence were infected with MVA-T7 (52) at a multiplicity of infection (MOI) of 1. After overnight incubation, both cell populations were mixed. Two hours later, the cells were lysed using Bright Glo lysis buffer (Promega), and the luciferase activity was determined using a luminescence counter (PerkinElmer Life Sciences) and the Britelite reporter gene assay system (PerkinElmer Life Sciences).

Compound *N*-(3-cyanophenyl)-2-phenylacetamide (3g) was synthesized and kindly provided by G. Hiltensperger and U. Holzgrabe, Institute of Pharmacy and Food Chemistry, University of Würzburg, Germany.

F/H coimmunoprecipitation. At 24 h posttransfection, the cells were washed three times with cold phosphate-buffered saline (PBS) and treated with the cross-linker DTSSP (3,3′-dithiobis-sulfosuccinimidyl propionate [1 mM final concentration in PBS]) for 2 h at 4°C, followed by addition of Tris (pH 7.5), to a final concentration of 20 mM for quenching (15 min, 4°C). Cells were subsequently lysed in radioimmunoprecipitation assay (RIPA) buffer (10 mM Tris [pH 7.4], 150 mM NaCl, 1% deoxycholate, 1% Triton X-100, 0.1% sodium dodecyl sulfate [SDS]) containing protease inhibitors (Roche complete mix) for 20 min on ice. Cleared lysates (20,000 × *g*, 20 min, 4°C) were incubated for 2 h with a mixture of three anti-CDV H MAbs (1C42H11 [VMRD], 2267, and 3900) (53) or with a mixture of three anti-MeV-H monoclonal antibodies (I41, I44, and 16DE6, kindly provided by M. Ehnlund) followed by overnight incubation with immunoglobulin G-coupled Sepharose beads. The pre-

cipitates were washed three times each in coimmunoprecipitation buffer followed by addition of 2× Laemmli sample buffer (Bio-Rad) containing 100 mM dithiothreitol. The samples were then subjected to Western blot analysis as previously described using either the polyclonal anti-H or the anti-F antibody (49, 51).

Flow cytometry. To determine the expression and conformation of the various F proteins specifically at the cell surface, Vero cells were transfected with 1 μg of F expression plasmids. One day posttransfection, unfixed and unpermeabilized cells were washed twice with ice-cold PBS and subsequently stained with one of the various MAbs (1:1,000) for 1 h at 4°C. The anti-CDV F MAbs 4941 (antiprefusion) and 4068 (antitrigger) or anti-MeV F MAbs 186CA (antiprefusion) and 19GD6 (antitrigger) were previously described as conformation-sensitive MAbs (37), whereas the anti-FLAG MAb (Sigma) was used to control for total cell surface expression (37). This was followed by intensive washes with ice-cold PBS and incubation of the cells with Alexa Fluor 488-conjugated secondary antibody (1:500) for 1 h at 4°C. Cells were washed 2 times with ice-cold PBS and consequently detached from the wells by adding PBS-EDTA (50 μM) for 30 min at 37°C. The mean fluorescence intensity (MFI) of 10,000 cells was then measured by using a BD LSRII flow cytometer (Becton, Dickinson).

RESULTS

A single V447T substitution in CDV F results in efficient triggering of CDV F by MeV H. Almost 20 years ago, Wild and colleagues identified a region of about 40 residues in CDV F (Onderstepoort vaccine strain) that, once mutated into the corresponding segment of MeV F, could restore membrane fusion activity in $CD46^+$ cells when combined with MeV H (MeV H/CD46). It was therefore speculated that this F region may act as an H-binding domain (34).

Since the strain origin reportedly determines productive heterotypic interaction of MeV and CDV glycoproteins (29), we first investigated whether restored fusion was restricted to CDV F derived from the vaccine strain. We exchanged the corresponding region in the F gene of the wild-type A75/17 CDV isolate with that of MeV F (Edmonston strain) (Chim 1) (Fig. 1A). In $CD46^+$ Vero cells, no cell-to-cell fusion was detectable when wild-type CDV F was combined with MeV H (not shown). In contrast, fusion activity was efficiently restored when Chim 1 was combined with MeV H in the Vero cell background (Fig. 1B). We thus generated three additional F chimeras, systematically narrowing the swapped MeV F section (Chim 2 to 4) (Fig. 1A). All three additional constructs were able to induce fusion when coexpressed with MeV H (Fig. 1B). Compared to the standard CDV F protein, Chim 4 carries 6 mutations (Fig. 1C) that are, based on our CDV F prefusion structural model, flanked by two cysteines engaged in an intramonomer disulfide bridge (C446 and C455) (Fig. 1D and E). We refer to this CDV F 446–455 microdomain as the "cysteine loop." This loop forms one side of a central pocket in the F globular head domain and stands in direct physical contact with a neighboring monomer (Fig. 1E). To further define which amino acid or acids are responsible for the observed gain of function, six single F mutants were prepared. Of these, only F-V447T could substantially restore fusion activity, as demonstrated qualitatively and quantitatively (Fig. 1F and G).

Cell surface expression and the conformational state of the individual F variants were next investigated by flow cytometry, using bioactive F trimers harboring an engineered FLAG tag in their ectodomain (37) and our recently identified pair of conformation-sensitive monoclonal antibodies (MAbs) that discriminate between prefusion and triggered F structures (37). All F mutants were expressed in the absence of H in Vero cells. Surface expression and folding into the prefusion conformation were essentially unchanged compared to those of the standard F in all mutants (Fig. 1H). These results indicate that under physiological conditions, no major conformational difference is appreciable between fusion-competent and noncompetent F variants.

Wild and colleagues previously also suggested that restoration of fusion activity might correlate with rescued F-H functional interactions (34). To address this question experimentally, we conducted coimmunoprecipitation (co-IP) experiments following a previously established procedure (54, 55) that we adapted from Paal and colleagues (30). The results shown in Fig. 1I indicate that CDV F-wt and the set of mutants efficiently bound MeV H. When coimmunoprecipitation efficiency was normalized for surface levels of H and F, no significant differences in physical interaction with H was observed between the F mutants (Fig. 1J). In addition, cleavage efficiency remained mostly unaltered for all mutants compared to that of F-wt (Fig. 1I).

Taken together, these results demonstrate that the valine-to-threonine substitution at CDV F position 447 was sufficient to restore fusion induction when combined with MeV H. Since this exchange did not substantially alter strength of physical interaction of CDV F with MeV H, restoration of membrane fusion must be controlled by another factor.

The CDV F-V447T variant exhibits unaltered fusion activity when combined with CDV H. We next investigated the capacity of the six single CDV F mutants to induce membrane fusion under CDV homotypic conditions in receptor-positive Vero-cSLAM cells. The fusion activities of all F mutants remained similar to that found for standard F (Fig. 2A and B). In agreement with this notion, assessment of F-H avidity revealed mostly unaltered coimmunoprecipitation efficiency compared to that of standard CDV F-H pairs (Fig. 2C and D).

Hence, cell-to-cell fusion induced by the CDV F-V447T variant combined with CDV H proceeded unperturbed in Vero-cSLAM cells, despite that fact that this mutation also enabled efficient fusion of $CD46^+$ cells when coexpressed with MeV H. These data demonstrate that restoration of membrane fusion by the 447T substitution in the CDV F cysteine loop microdomain did not result from a restored physical interaction of heterotypic CDV F and MeV H, as previously suggested by Wild and colleagues (34). Rather, our findings are consistent with the idea that efficient MeV H-dependent CDV F-V447T triggering is regulated by a novel mechanism.

Alanine substitutions within the F cysteine loop do not impede cell-to-cell fusion. We next determined whether alanine substitutions of the six positions in the cysteine loop that differ between CDV and MeV F affect membrane fusion activity in a receptor- and H-dependent manner. First, we expressed the alanine-substituted F variants in Vero cells together with MeV H. (The naturally present alanine residue at position 453 was changed to serine.) Under these experimental conditions, none of the mutated F trimers restored fusion activity (Fig. 3B). Probing of cell surface expression and the F conformational state indicated that all F mutants assumed a metastable prefusion state, but F-A453S and F-I454A showed substantial reductions in cell surface expression (Fig. 3A). Physical interaction of F mutants with MeV H was not significantly altered in any of these F mutants (Fig. 3C and D).

When these experiments were repeated with CDV H in Vero-

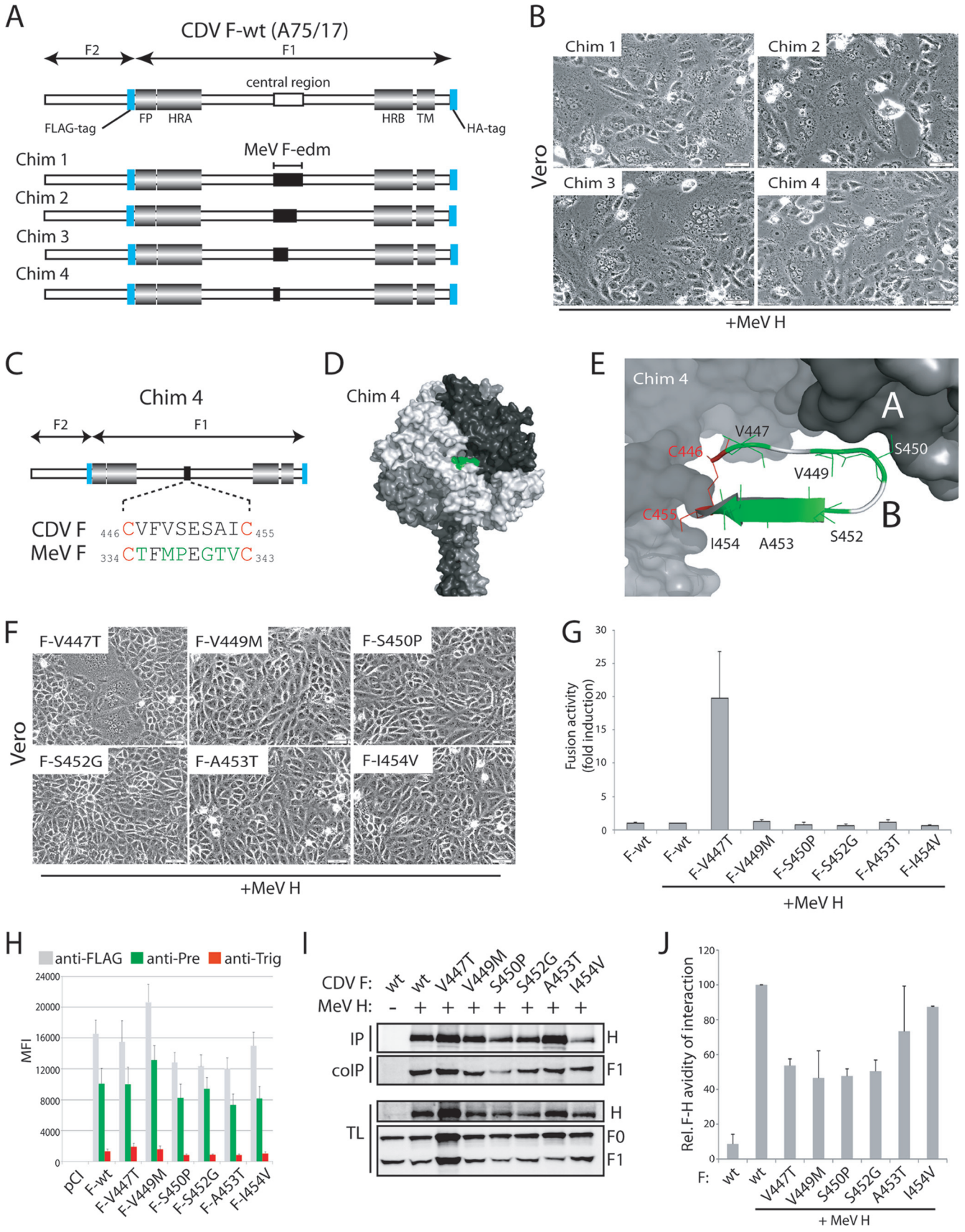
A
CDV F-wt (A75/17)
F2
F1
central region
FLAG-tag
FP
HRA
HRB
TM
HA-tag
MeV F-edm
Chim 1
Chim 2
Chim 3
Chim 4
B
Chim 1
Chim 2
Chim 3
Chim 4
Vero
+MeV H
C
Chim 4
F2
F1
CDV F 446 CVFVSESAIC 455
MeV F 334 CTFMPEGTVC 343
D
Chim 4
E
Chim 4
A
B
V447
C446
S450
V449
C455
I454
A453
S452
F
F-V447T
F-V449M
F-S450P
F-S452G
F-A453T
F-I454V
Vero
+MeV H
G
Fusion activity (fold induction)
F-wt
F-wt
F-V447T
F-V449M
F-S450P
F-S452G
F-A453T
F-I454V
+MeV H
H
anti-FLAG
anti-Pre
anti-Trig
MFI
pCI
F-wt
F-V447T
F-V449M
F-S450P
F-S452G
F-A453T
F-I454V
I
CDV F:
MeV H:
wt
wt
V447T
V449M
S450P
S452G
A453T
I454V
IP
coIP
TL
H
F1
F0
J
Rel. F-H avidity of interaction
F:
wt
wt
V447T
V449M
S450P
S452G
A453T
I454V
+ MeV H

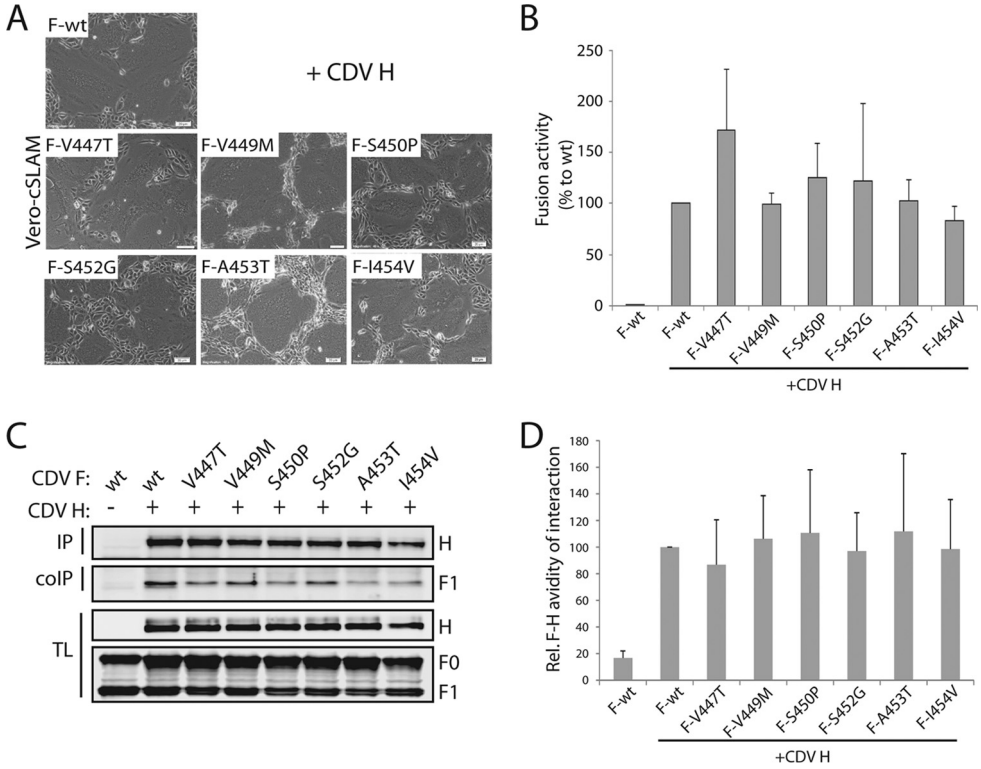

FIG 2 Microdomain-mutated CDV F proteins remained fully active when combined with CDV H. (A) Syncytium formation assay. Cell-cell fusion induction after cotransfection of Vero-cSLAM cells with plasmid DNAs encoding various CDV F proteins and CDV H. Representative fields of view were captured with a confocal microscope (Olympus FluoView FV1000) 24 h posttransfection. (B) Quantitative cell-cell fusion assay. Fusion activity was quantitatively assessed as described in the legend to Fig. 1G. (C) Assessment of H interaction with functional F proteins. Co-IPs were performed as described in the legend to Fig. 1I, with the exception of the MAbs used (1C42H11, 3900, and 2267). (D) Semiquantitative assessment of F-H avidity of interaction. The strengths of F-H interactions were calculated as described in the legend to Fig. 1J.

cSLAM cells, we found that all F alanine variants efficiently induced cell-cell fusion, although to a lesser degree for F-A453A and F-I454A (Fig. 3E). Assessment of the F-H strength of interactions again indicated wild-type-like H-binding efficiency of the F mutants (Fig. 3F and G). Taken together, these results confirmed that the cysteine loop microdomain is not involved in short-range interaction with H: rather, our data underline a key role of the CDV F residue 447 in regulating heterotypic fusion after coexpression with MeV H.

FIG 1 A microdomain in the F head domain controls fusion without influencing interactions with H. (A) Scheme of the morbillivirus F gene. Conserved regions among class I fusion proteins are shown for the fusion peptide (FP), heptad repeat regions A and B (HRA and HRB), and transmembrane domain (TM). The blue boxes represent the position along the gene selected for FLAG and HA epitope insertions. The region in the CDV F (A75/17) swapped by the corresponding region in MeV F (Edmonston) is shown in black. (B) Syncytium formation assay. Cell-cell fusion induction after cotransfection of Vero cells with plasmid DNAs encoding various CDV F proteins and MeV H. Representative fields of view were captured with a confocal microscope (Olympus FluoView FV1000) 24 h posttransfection. (C) Highlight of the amino acid differences between CDV F and Chim 4. (D) Homology model of the prefusion CDV F trimer (49); the segment from positions 446 to 455 in CDV F is shown in green. (E) Close-up view of the microdomain in the CDV F that controls fusion (referred to as the "cysteine loop"). (F) Syncytium formation assay. Cell-cell fusion was performed as described in panel B but with single CDV F mutants. (G) Quantitative fusion assay. Target Vero cells, Vero-cNectin-4 cells, or Vero-cSLAM cells (as indicated) were infected with MVA-T7 (MOI of 1). In parallel, another population of Vero or CHO cells (effector cells) was transfected with the different F proteins, the indicated H protein, and a plasmid containing the luciferase reporter gene under the control of the T7 promoter. Twenty hours after transfection, effector cells were mixed with target cells and seeded into fresh plates. After 2 h at 37°C, fusion was indirectly quantified by using a commercial luciferase-measuring kit. For each experiment, the value obtained for the standard F-H combination was set to 1. Means of three independent experiments in duplicate are shown. (H) Surface expression and F conformational state probing. Vero cells were transfected with the F expression plasmids mentioned above. For immunofluorescence (IF) analysis, cells were stained with the different anti-F MAbs (FLAG [gray bars], 4941 [green bars], and 4068 [red bars]) 24 h posttransfection at 4°C. Alexa Fluor 488-conjugated secondary antibody was then added, and stained cells were subjected to flow cytometry to record mean fluorescence intensities (MFI). Means of three independent experiments performed in duplicate are shown. (I) Assessment of H interaction with functional F proteins. To stabilize the F-H interactions, transfected Vero cells were treated with DTSSP. MeV H- and CDV F-coexpressing Vero cells were then lysed with RIPA buffer, and complexes were immunoprecipitated (IP) with three anti-H MAbs (I41, I44, and 16DE6) and protein G-Sepharose bead treatment. Proteins were boiled and subjected to immunoblotting using a polyclonal anti-HA antibody to detect the F antigenic materials. Co-IP F proteins were detected in comparison with F present in the lysates prior to IP by immunoblotting using a polyclonal anti-F antibody (TL, total lysate; F_0, uncleaved F protein; F_1, cleaved membrane-anchored F subunit). For a control, total H proteins, obtained by direct immunoprecipitation with the above-mentioned MAbs, were revealed by immunoblotting using a polyclonal anti-H antibody (IP). (J) Semiquantitative assessment of F-H avidity of interaction. To quantify the avidities of F_1-H interactions, the signals in each of the F_1 and H bands were quantified using the AIDA software package. The avidity of F_1-H interactions is represented by the ratio of the amount of coimmunoprecipitated F_1 over the product of F_1 in the cell lysates divided by the ratio of the amount of immunoprecipitated H over the product of H in the cell lysate. Subsequently, all ratios were normalized to the ratio of the wild-type F-H interactions set to 100%. Averages represent at least two independent experiments.

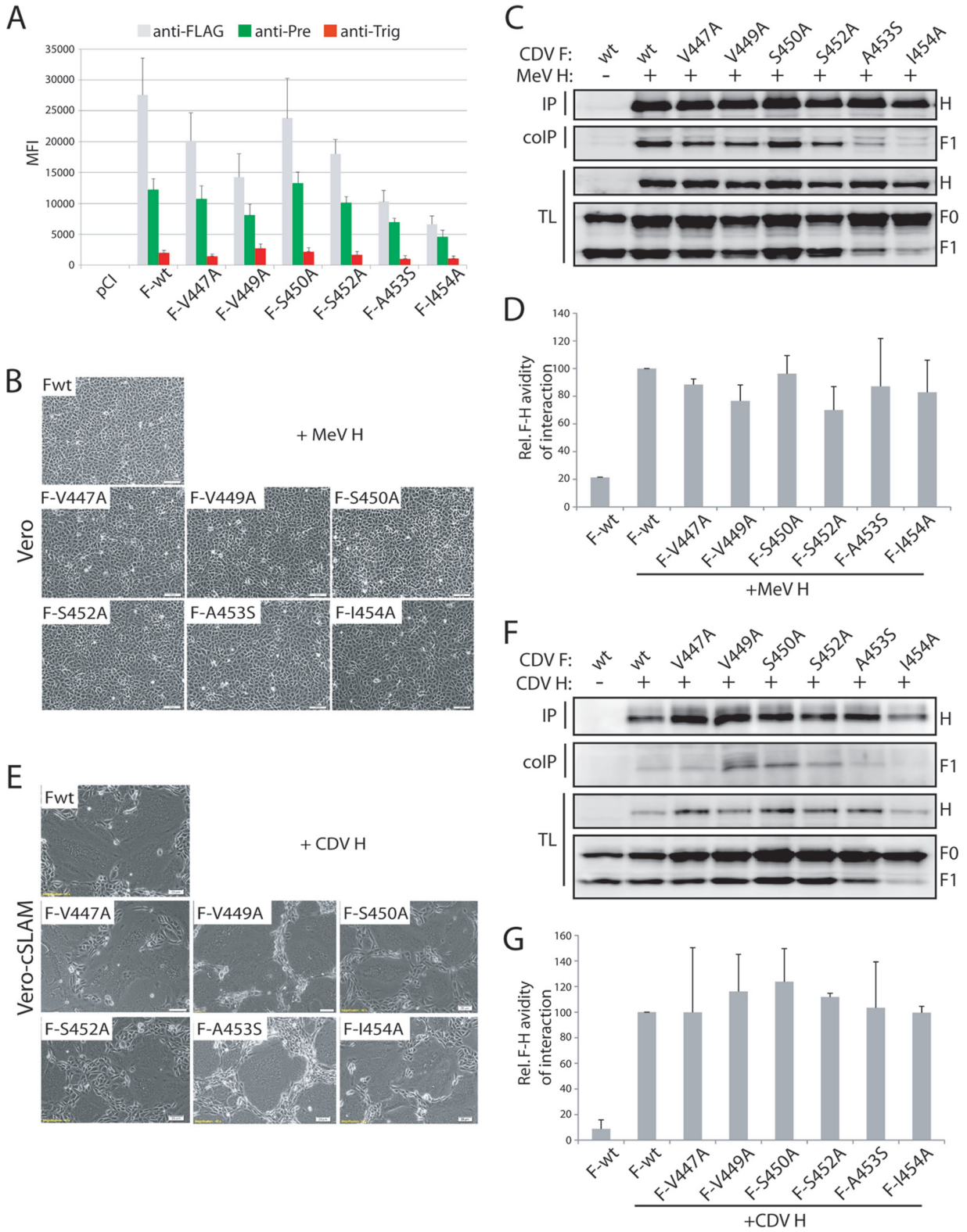

FIG 3 Effect on cell-cell fusion of alanine substitutions within the F trimer's cysteine loop microdomain. (A) Surface expression and F conformational state probing. Immunofluorescence (IF) and flow cytometry were performed as described in the legend to Fig. 1H. anti-Pre, antiprefusion; anti-Trig, antitrigger. (B and E) Syncytium formation assay. Shown is cell-cell fusion induction after cotransfection of Vero or Vero-cSLAM cells with plasmid DNAs encoding various F proteins and H proteins (as indicated). Representative fields of view were captured with a confocal microscope (Olympus FluoView FV1000) 24 h posttransfection. (C and F) Assessment of H interaction with functional F proteins. Co-IPs were performed as described in the legend to Fig. 1I or 2H. (D and G) Semiquantitative assessment of F-H avidity of interaction. The strengths of F-H interactions were calculated as described in the legend to Fig. 1J.

The conformational stability of the V447T F trimer is reduced. We recently provided evidence that morbillivirus H proteins trigger F by actively altering the activation energy barrier because morbillivirus F trimers are capable of maintaining a metastable prefusion conformation in the absence of H (37).

To test the conformational stability of prefusion F trimers harboring mutations at position 447 in the cysteine loop, we expressed standard F, F-V447T, and F-V447A in Vero cells in the absence of H. Subsequently, cells were briefly heat shocked at 40, 50, 54, and 60°C, respectively, and the stability of each F variant was assessed using the conformation-sensitive MAbs. Strikingly, F-V447A exhibited 50% of postfusion trimers only at 54°C, while F-V447T started to switch conformation already at 50°C (Fig. 4A). In contrast, standard F trimers were still substantially in the prefusion conformation even at 60°C (Fig. 4A). These data suggest that the V447T substitution in CDV F decreased the activation energy barrier for F activation.

To validate these data, we coexpressed F-V447T and Chim 4 (carrying all 6 mutations) with CDV H in Vero-cSLAM cells and incubated the cells at physiological or reduced temperature. Both F variants were still able to induce cell-to-cell fusion even at 25°C, while standard F showed essentially no fusion at this temperature (Fig. 4B).

Taken together, our data reveal that the V447T substitution in CDV F destabilized the prefusion F trimers, which set the stage for productive triggering by a heterotypic attachment protein.

In MeV F, the residue homologous to CDV F position 447 determines the stability of the prefusion conformation. We next determined whether the homologous residue in MeV F (T335) likewise serves as a determinant for prefusion F conformational stability (Fig. 5A). To test this, we mutated this residue to alanine and valine. Both F variants were properly surface expressed and recognized efficiently by the prefusion F-specific MAb (Fig. 5B). Interestingly, cell-to-cell fusion assays revealed reduced bioactivity for both F mutants, independent of the origin of the H protein used for triggering (Fig. 5C and D). Assessment of the avidity of the F-H interaction indicated very similar physical binding of all three F trimers to H, confirming that the cysteine loop microdomain of MeV F is not involved in short-range interactions with H tetramers (Fig. 5E to H). However, an assessment of the conformational stabilities of these mutant prefusion MeV F trimers revealed that both variants were slightly more stable than standard MeV F; more F-T335V and F-T335A prefusion trimers were detected by the antiprefusion F MAb after exposure to 54°C than standard F trimers, and only standard MeV F showed approximately 50% conversion to the postfusion conformation at this temperature (Fig. 5I).

Overall, these data confirm that (i) the cysteine loop in morbillivirus F proteins is not a direct H contact zone, and (ii) the nature of the residue at the homologous positions 335 (in MeV F) and 447 (in CDV F) in the cysteine loop affects the conformational stability of the prefusion F trimers. Under suboptimal F-triggering conditions (i.e., the heterotypic combination of CD46 with MeV H), only the destabilized mutant F trimers are efficiently activated.

The central pocket microdomain rather than the cysteine loop governs the conformational stability of CDV prefusion F. Structural models of paramyxovirus prefusion F trimers posit each of the three cysteine loop microdomains in physical contact with an adjacent monomer. Interestingly, we previously obtained evidence for another residue within the CDV F trimer

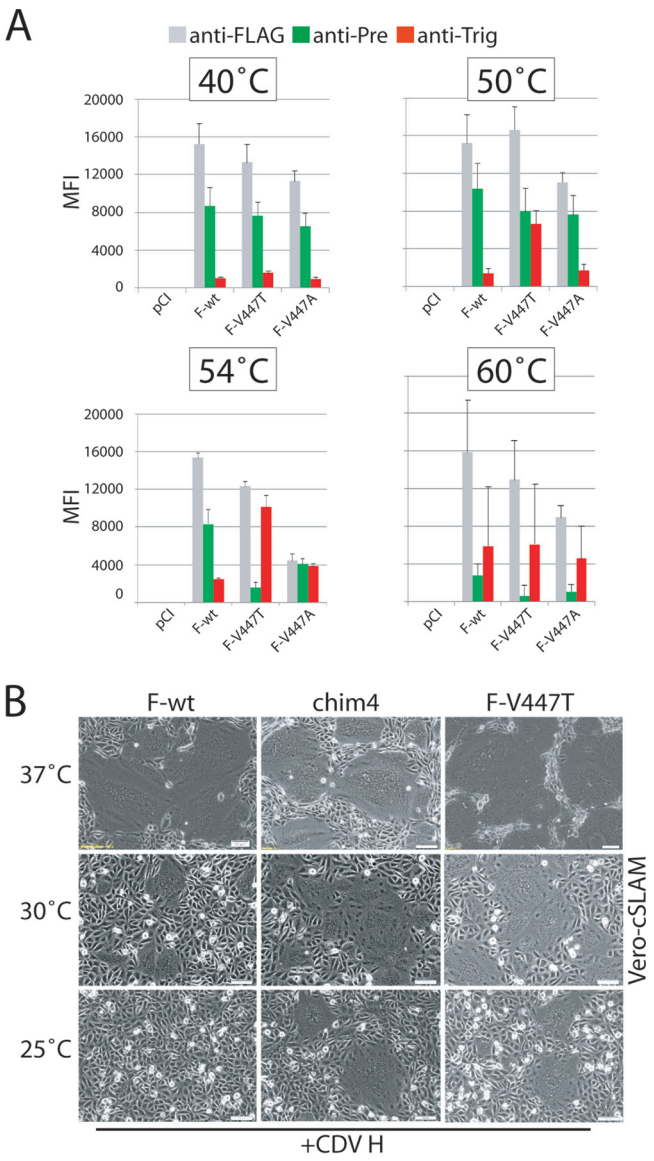

FIG 4 Investigation of the conformational stability of prefusion CDV F variants. (A) Vero cells were transfected with standard- or variant-expressing plasmid DNA. Immunofluorescence (IF) and flow cytometry were performed as described in the legend to Fig. 1H. In some experiments, brief heat shocks (10 min at the indicated temperatures) were performed prior to IF. (B) Syncytium formation assay. Cell-cell fusion induction after cotransfection of Vero-cSLAM cells with plasmid DNA encoding mutant CDV F proteins and CDV H. In some experiments, the cells were incubated overnight at 30 or 25°C. Representative fields of view were captured with a confocal microscope (Olympus FluoView FV1000) 24 h (30°C) or 48 h (25°C) posttransfection.

(L372) that, when mutated into an alanine or glycine, also significantly reduced the activation energy barrier of metastable F (49). Strikingly, the structural model places CDV F-L372 and -V447 in very close proximity, thereby inferring that this domain at large, rather than an individual residue, controls the conformational stability of prefusion F (Fig. 6A). To further investigate this notion, we mutated residues on the opposite monomer that are predicted to establish close contacts with L372 and V447. Three candidate residues were selected (L326, P331, and S332) and subsequently replaced with alanine (Fig. 6A). Remarkably, CDV F-L326A and F-P331A (but not

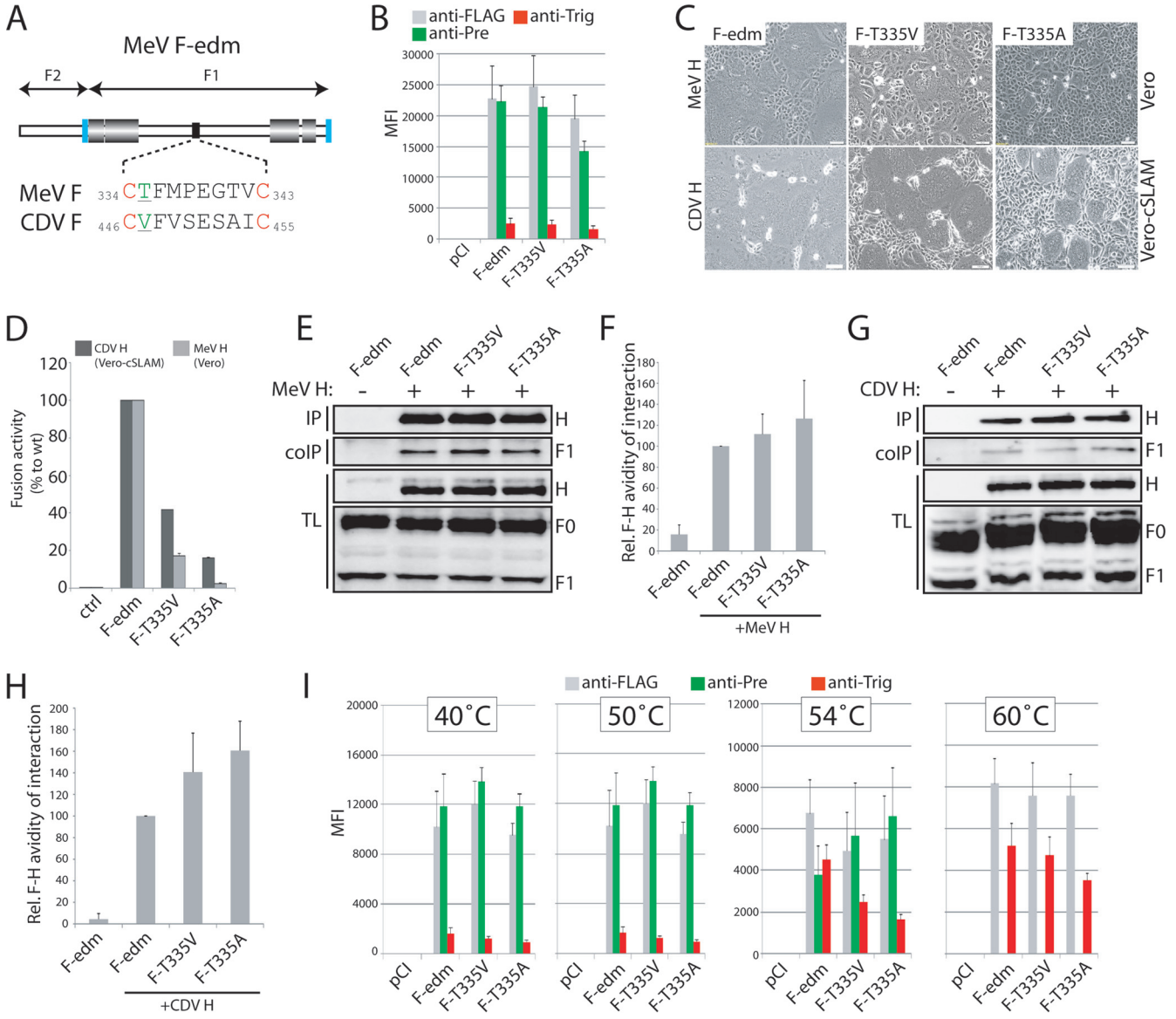

FIG 5 Stabilization of prefusion MeV F-Edm trimers. (A) Scheme of the morbillivirus F gene and highlight of the amino acid differences between MeV F and CDV F in the central region (black box). (B) Surface expression and F conformational state probing. Immunofluorescence (IF) and flow cytometry were performed as described in the legend to Fig. 1H, with the exception of the conformation-sensitive MAbs used (anti-MeV F 186CA and 19GD6). (C) Syncytium formation assay. Shown is cell-cell fusion induction after cotransfection of Vero or Vero-cSLAM cells with plasmid DNA encoding mutant MeV F proteins and either MeV H or CDV H. Representative fields of view were captured with a confocal microscope (Olympus FluoView FV1000) 24 h posttransfection. (D) Quantitative cell-cell fusion assay. Fusion activity was quantitatively assessed as described in the legend to Fig. 1G. (E and G) Assessment of H interaction with functional F proteins. Co-IPs were performed as described in the legend to Fig. 1I, with the exception of the MAbs used for IP (anti-MeV H I41, I44, and 16DE6). (F and H) Semiquantitative assessment of F-H avidity of interaction. The strengths of F-H interactions were calculated as described in the legends to Fig. 1J and 2H. (I) Investigation of the thermal stabilities of the various F variants. Vero cells were transfected with standard- or variant-expressing plasmid DNA. Immunofluorescence (IF) and flow cytometry were performed as described in the legend to Fig. 1H. In some experiments, brief heat shocks (10 min at the indicated temperatures) were performed prior to IF.

F-S332A) efficiently restored cell-to-cell fusion when combined with MeV H in CD46-expressing Vero cells and subjected to qualitative and quantitative assays (Fig. 6B and C).

When the temperature dependence of F refolding was assessed, we found that all of these CDV F variants were destabilized compared to standard F (Table 1). We also noted that the CDV F-S332A variant, although destabilized, was the only trimer that reproducibly exhibited reduced fusion in Vero-cSLAM cells (Fig. 7A and B). We propose that this F mutant is very likely impaired by one or multiple additional steps required for productive fusion pore formation.

F trimers with a mutated central pocket are resistant to inhibition by the AS-48 class of morbillivirus membrane fusion inhibitors. Plemper and colleagues reported the development of a very potent antiviral against MeV (42, 43, 45), a molecule subsequently shown to also be very effective against CDV (44). Doyle et al. and Prussia et al. demonstrated that intracellular transport competence of some escape mutants became dependent on the

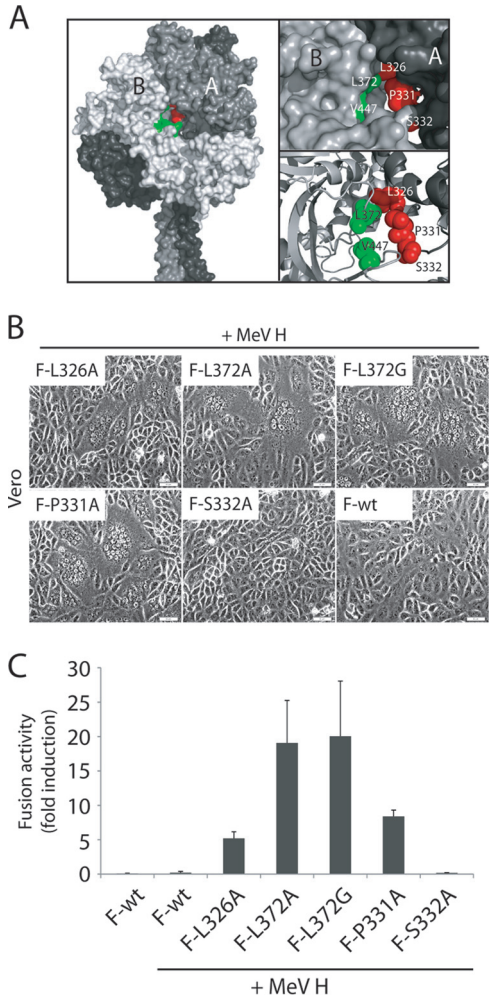

FIG 6 A central pocket microdomain within the F head regulates cell-cell fusion. (A) (Left panel) Homology model of the prefusion CDV F trimer (49). The central pocket is highlighted (green, monomer B; red, monomer A). (Right panel) Close-up view of residues defining the central microdomain. (Residues in the monomer B are color coded green, and residues in monomer A are color coded red). (B) Syncytium formation assay. Cell-cell fusion induction after cotransfection of Vero cells with plasmid DNA encoding mutant CDV F proteins and MeV H proteins. Representative fields of view were captured 24 h posttransfection with a confocal microscope (Olympus FluoView FV1000). (C) Quantitative cell-cell fusion assay. Fusion activity was quantitatively assessed as described in the legend to Fig. 1G.

drug, and several resistant F variants showed a hyperfusogenic phenotype (45, 46). These results strongly suggested that mutant F trimers resisted the AS-48 compound by a mechanism other than prevention of direct docking of the molecule. We recently found that a member of this inhibitor class, 3g, stabilized a conformation of the F trimer that is recognized by the antiprefusion antibody, hence precluding H-mediated F triggering (37). Interestingly, substitutions in previously generated AS-48-resistant F mutants differ from those identified in the present study (45). We therefore hypothesized that the F mutants designed in this study and those previously reported all induce secondary resistance through destabilization of prefusion F trimers, rather than primary site resistance.

To test this concept, standard and mutants CDV F trimers were coexpressed with CDV H in SLAM-positive Vero cells in the presence or absence of a high concentration of 3g (50 μM). While membrane fusion was massive in the absence of the compound, 3g strongly inhibited fusion activity of standard F and H complexes (Fig. 7A, B, and C). In contrast, cell-to-cell fusion was still substantial in the presence of 3g when CDV H was combined with the destabilized F trimers (with the exception of F-S332A) (Fig. 7A, B, and C).

To differentiate between secondary resistance to fusion inhibition resulting from insufficient stabilization of mutant prefusion F trimers and primary site loss of 3g binding, we probed whether the compound still exerted some effect by enhancing the temperature at which mutated F trimers switched conformations. Standard and selected mutant F proteins were expressed in Vero cells and subjected to conformational analysis of F trimers after brief heat shocks as before. Strikingly, all tested mutant F trimers flipped from the pre- to postfusion conformation at higher temperatures in the presence of 3g than in its absence (Table 1). These data indicate that the compound still stabilized most of the CDV prefusion F variants to some appreciable degree (Table 1).

Taken together, we demonstrate that only destabilized, mutant prefusion F complexes, efficiently escape from inhibition by the compound. These findings are consistent with secondary resistance to the inhibitor.

The nature of the fusion trigger and the stability of metastable prefusion F control productive fusion activation. Only destabilized CDV F trimers were activated by the MeV H/CD46 trigger, whereas both standard and modified CDV F proteins were triggered by the CDV H/cSLAM interaction. Although it is well known that the cellular environment regulates paramyxovirus-mediated membrane fusion (5), our findings in addition suggest that fusion is controlled by the nature of the combination (receptor type and H origin) involved in triggering. We tested the effect of different fusion-triggering combinations by expressing standard CDV H proteins with standard or mutated CDV F trimers in Vero cells displaying either cSLAM or cNectin-4. Importantly, since the cell surface steady-state level of the receptor also impacts membrane fusion activity (56), the levels of surface expression of both cSLAM and cNectin-4 were monitored by flow cytometry. (Both molecules carry identical extracellular HA tags.) The results indicated that our newly generated Vero-cNectin-4 cells expressed slightly more receptors on the plasma membrane than Vero-cSLAM cells (Fig. 8).

Results shown in Fig. 9 revealed that all F proteins induced membrane fusion in the absence of 3g in Vero-cNectin-4 cells, albeit to a lesser degree than in Vero-cSLAM cells (compare

TABLE 1 Prefusion F protein stability of CDV

CDV	Temp of conformation switch (°C)[a]	
	No drug	+3g
F-wt	58–60	65–67
F-L326A	50–52	60–62
F-L372G	44–46	51–53
F-L372A	51–53	60–62
F-P331A	50–52	60–62
F-S332A	50–52	60–62
F-V447T	51–53	61–63

[a] Determined by detecting the temperature at which 50% of the F population was bound by the antiprefusion MAb and the other 50% was bound by the antitrigger MAb.

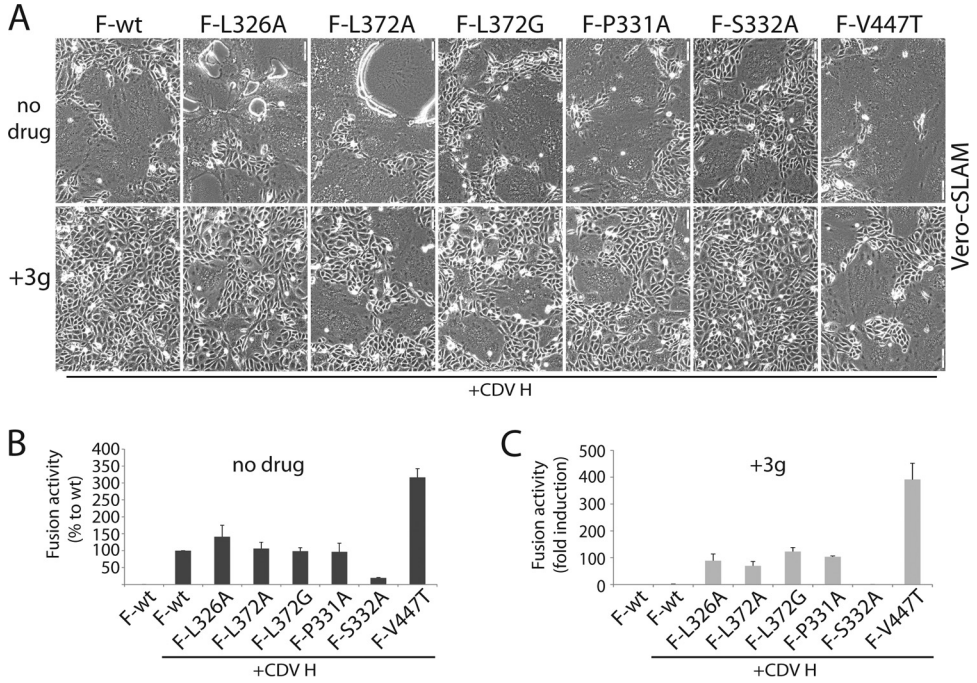

FIG 7 Prefusion F trimers with reduced activation energy levels are resistant to a potent morbillivirus cell entry inhibitor (3g). (A) Syncytium formation assay. Cell-cell fusion induction after cotransfection of Vero-cSLAM with plasmid DNA encoding F proteins and H proteins in different combinations (as indicated in the figure) in the absence (no drug) or presence (+3g) of the antiviral compound. Representative fields of view were captured with a confocal microscope (Olympus FluoView FV1000) 24 h posttransfection. (B and C) Quantitative cell-cell fusion assay. Fusion activity was quantitatively assessed as described in the legend to Fig. 1G.

Fig. 7A and 9A). Consistent with the results obtained in Vero-cSLAM cells, only F-S332A failed to fuse Vero-cNectin-4 cells, confirming that this particular mutation disturbs basic functionality of the F trimer through additional defects (Fig. 9A and B). In contrast to the results obtained in Vero-cSLAM cells, only F-L372G could mediate fusion in the presence of 3g. However, induction of fusion by this mutant was extremely limited and was detectable only qualitatively after 48 h of incubation (Fig. 9A). Interestingly, this CDV F mutant was also the only one that displayed a significantly reduced conformational stability of the prefusion trimer (Table 1).

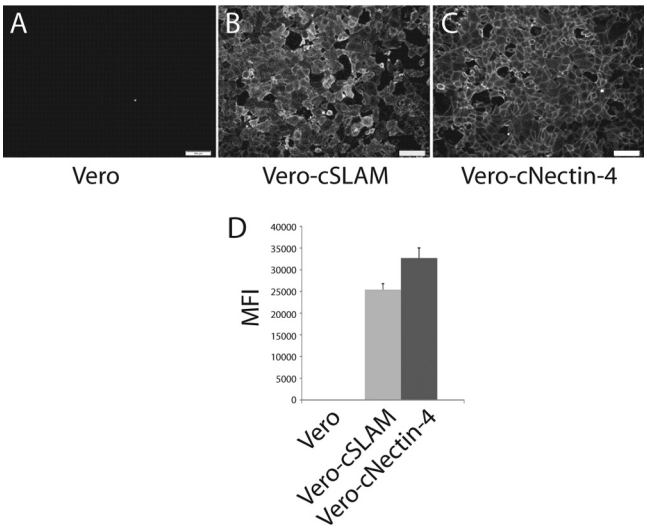

FIG 8 Generation of a stable Vero-cNectin-4 cell line. Vero cells were transduced with lentiviral vectors carrying the canine nectin-4 gene. The gene was designed to express a protein with the HA tag fused N terminally. IF (A to C) and flow cytometry (D) of Vero cells, Vero-cSLAM cells (SLAM also bears an additional N-terminal HA tag), and Vero-cNectin-4 cells were performed as described in Fig. 1H, with the exception of the primary antibody used (anti-HA 16B12).

Overall, these results confirmed that the receptor type influences the outcome of H-mediated F triggering. We extend this notion by revealing that both the nature of the triggering system and the conformational stability of the prefusion F trimers govern the productive initiation of the F refolding cascade and, by extension, the sensitivity of the system to 3g-mediated inhibition.

Low stability of prefusion F trimers generates inhibitor-dependent F proteins. Previous (37) and current results support the notion that 3g inhibits membrane fusion by stabilizing a prefusion conformation of the F trimer. In contrast to standard F complexes, however, destabilized CDV F mutants efficiently escape from inhibition, and in the MeV F background, resistance to the compound was associated with a hyperfusogenic phenotype (46).

To further assess a link between F stability and resistance to 3g, we coexpressed a reportedly extremely labile MeV F variant (F-L547A V549A) (37) with MeV H in Vero cells. Indeed, fusion was nearly absent, since most F trimers reached the cell surface already in a postfusion conformation ("dead" F) (37). We hypothesized that membrane fusion might be restored if the stability of the F trimers could be appropriately influenced by the compound: high enough to preclude premature refolding but sufficiently low to enable H-mediated F triggering (thus generating 3g-dependent

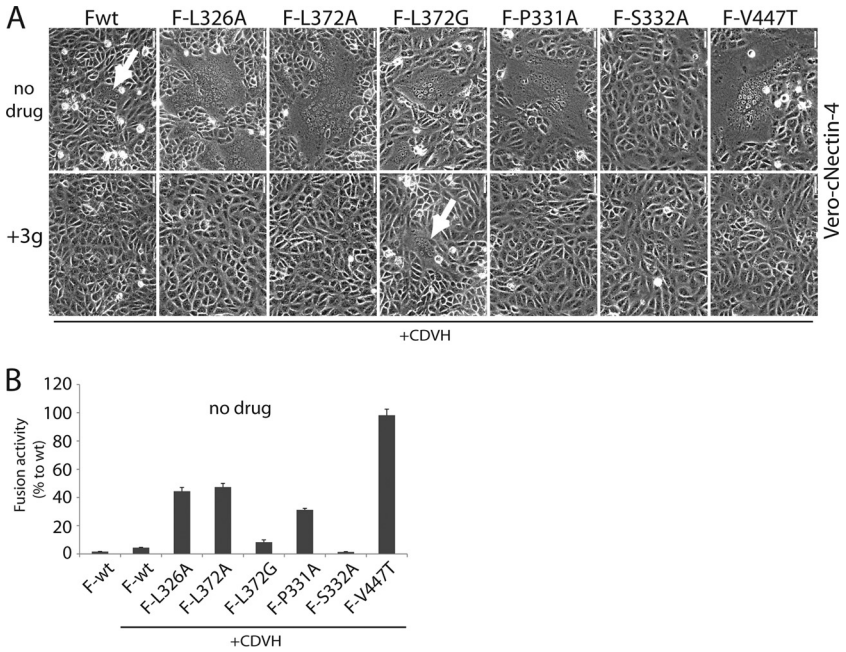

FIG 9 The triggering stimulus governs secondary resistance of various destabilized F variants to the antiviral compound. (A) Cell-cell fusion induction after cotransfection of Vero-cNectin-4 cells with plasmid DNA encoding CDV F and CDV H proteins in the absence (no drug) or presence (+3g) of the antiviral compound. Representative fields of view were captured with a confocal microscope (Olympus FluoView FV1000) 24 h (no drug [upper panels]) and 48 h (+3g [lower panels]) posttransfection. (B) Quantitative cell-cell fusion assay. Fusion activity was quantitatively assessed as described in the legend to Fig. 1G.

bioactive F trimers in analogy to the AS-48-dependent F-V94G N462S trimers previously reported [45]).

We found syncytia in Vero cells cotransfected with MeV H and F-L547A V549A in the presence of 3g (Fig. 10A and C), while fusion remained extremely low without the compound (Fig. 10A and B). This phenotype became even more pronounced when the destabilized MeV F variant was coexpressed with CDV H in Vero-cSLAM cells (Fig. 10D, E, and F). Remarkably, this result perfectly correlated with the conformational stability of the mutant prefusion F trimer: while F-L547A V549A flipped at approximately 33 to 35°C in the absence of 3g, it switched conformations at 42 to 44°C in the presence of the compound (Table 2). Thus, also the combination of the L547A and V549A substitutions resulted in 3g-dependent functional MeV F trimers.

DISCUSSION

To enter target cells, morbilliviruses first interact with specific host cell receptors through their envelope attachment protein H (5). The ensuing receptor-induced oligomeric rearrangements within the H tetramers trigger associated prefusion F trimers to undergo a series of irreversible conformational changes that ultimately result in membrane fusion (5). Our recent findings demonstrated that the conformational stability of morbillivirus prefusion F trimers does not rely on the presence of H but on an intrinsic activation energy barrier (37).

Based on previous work by Wild and coworkers (34), we here identified specific F residues located in neighboring monomers that define a recessed pocket positioned at the center of the large F globular head domain. When these residues were mutated to the corresponding MeV F amino acids in the CDV F background, membrane fusion of $CD46^+$ Vero cells was efficiently restored upon coexpression with MeV H. Interestingly, we show that this gain of function was not induced by restoring or improving F-H physical interactions but by lowering the activation energy barrier of metastable, prefusion CDV F trimers, hence facilitating H-dependent F triggering. In support of this concept, we recently found that vaccine strain (Edmonston)-derived MeV F contains a substantially lower activation energy barrier than CDV F (A75/17), as monitored by heat shock treatment and conformation-sensitive MAbs (37). This finding implies that the stimulus provided by CD46-induced conformational changes of MeV H is strong enough to overcome the relatively low energy barrier of prefusion MeV F-Edm but insufficient to trigger the more stable CDV F complexes. In the present study, we demonstrate that mutations in the central pocket domain of the F head reduce the activation energy barrier of prefusion CDV F complexes, allowing for efficient triggering also by MeV H/CD46. These conclusions are supported by the resistance of the destabilized F trimers to the small-molecule entry inhibitor that blocks fusion by stabilizing a prefusion state of F. A still appreciable F stabilization in refolding assays supports that resistance was based on a secondary mechanism, and the compound still bound to F.

A regulatory role of destabilizing F mutations and the cellular system was suggested in several studies to modulate the efficiency of the fusion process (45, 49, 57–59). Based on the results presented in this study, we propose that the receptor type, the strain origin of the attachment protein, and the conformational stability of the prefusion F trimers all cooperate to define the framework for membrane fusion activation. First, if the stability of prefusion F trimers is too high, the triggering stimulus provided by H upon receptor binding will not suffice to overcome the F activation energy barrier; if the F stability is too low, F trimers will prematurely refold into the postfusion state. Metastable F trimers are only amenable to productive triggering if they contain activation energy

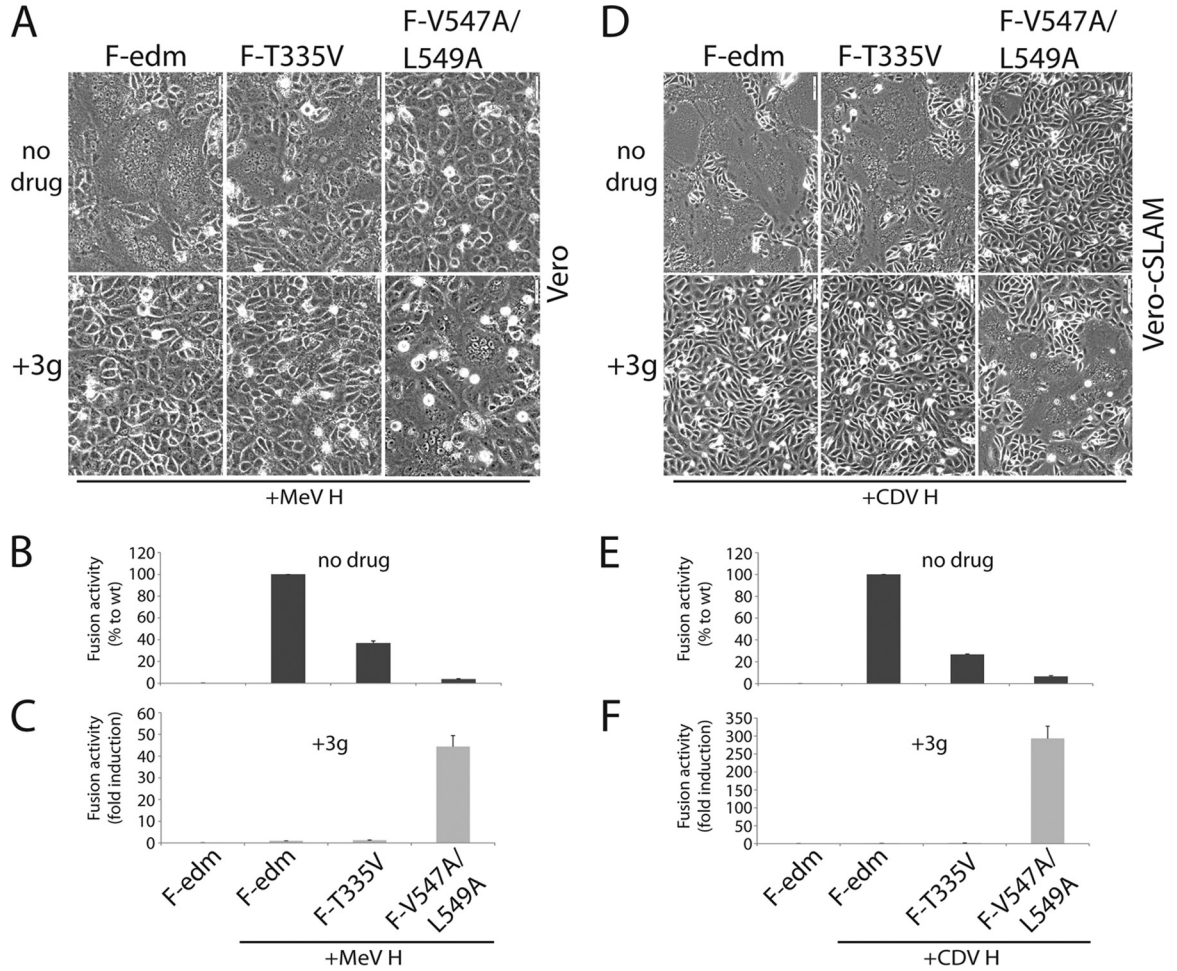

FIG 10 Identification of drug-dependent bioactive F trimers. (A and D) Syncytium formation assay. Shown is cell-cell fusion induction after cotransfection of Vero (A) or Vero-cSLAM (B) cells with plasmid DNA encoding F proteins and H proteins in different combinations (as indicated) in the absence (no drug) or presence (+3g) of the antiviral compound. Representative fields of view were captured with a confocal microscope (Olympus FluoView FV1000) 24 h posttransfection. (B and C and E and F) Quantitative cell-cell fusion assay. Fusion activity was quantitatively assessed as described in the legend to Fig. 1G.

levels between these two thresholds. We consider this energy range between these two thresholds the "triggering range" (Fig. 11A to C). Second, the breadth of the triggering range depends on the combination of the receptor type and the origin of the viral attachment protein, which we refer to as the "triggering stimulus." As a case in point, the MeV H/CD46 combination appears to be a suboptimal trigger, defined by a poor triggering stimulus: highly stable wt CDV F trimers (A75/17) resisted activation by this trigger, while MeV F-Edm (intrinsically less stable) and destabilized CDV F variants were activated (Fig. 11A). In contrast, the CDV H/cSLAM triggering stimulus is strong, reflected by a wide triggering range encompassing all F trimers tested in this study (Fig. 11B). The CDV H/cNectin-4 combination mounts an intermediate triggering stimulus, since CDV F-wt remained mostly untriggered, but MeV and destabilized CDV F trimers were effectively activated (Fig. 11C).

TABLE 2 Prefusion F stability of MeV

MeV	Temp of conformation switch (°C)[a]	
	No drug	+3g
F-edm	51–53	61–63
F-T335V	54–56	63–65
F-V547A L549A	33–35	44–46

[a] Determined by detecting the temperature at which 50% of the F population was bound by the antiprefusion MAb and the other 50% was bound by the antitrigger MAb.

Use of the small-molecule fusion inhibitor further accentuated this model. In the presence of 3g, the conformational stability of wt CDV F prefusion trimers increased beyond the threshold of activation, blocking membrane fusion at all triggering conditions. Remarkably, 3g increased the activation energy barriers of MeV and destabilized CDV F trimers to a similar range as untreated wt CDV F. This may explain why destabilized F mutants are resistant to inhibition by the compound when subjected to a strong triggering stimulus (CDV H/cSLAM). In contrast, under intermediate (CDV H/cNectin-4) or suboptimal (MeV H/CD46) triggering stimuli, only the most destabilized CDV F variant (L372G) still escapes from inhibition by 3g.

Strikingly, MeV F variants were reported that were able to efficiently grow in Vero cells in the presence of AS-48, the signature compound of this antiviral class and close chemical analog to 3g (45). These MeV variants exhibited mutated F trimers that were

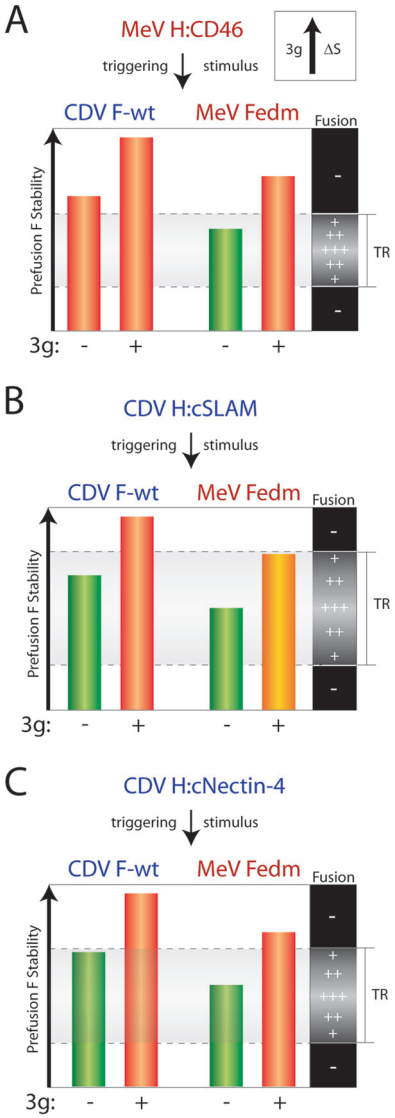

FIG 11 Refined model of receptor/H-dependent F triggering. (A to C) The histograms represent the stability of a given F trimer in the metastable state. The increase in stability of prefusion F states by 3g is shown in the upper insert (ΔS). "Triggering range" (TR) is defined by the receptor type, the strain origin of H, and the stability of a given prefusion F trimer. The MeV H/CD46 "stimulus" represents a suboptimal trigger (leading to a narrow TR). The CDV H/cNectin-4 "stimulus" represents an intermediate trigger (leading to an intermediate TR). The CDV H/cSLAM "stimulus" represents an optimal trigger (leading to a large TR). If the stability of a given prefusion F trimer is above the upper threshold or below the lower one, F refolding is not induced (red histogram, unamenable to triggering by H). If, in contrast, the stability is above the lower threshold and below the upper one, F refolding can be triggered (green histogram, amenable to triggering by H). In addition, we propose that within the TR the closer the stability to the upper or lower threshold, the less fusion is induced, thereby defining a range of potential fusion efficiencies (+, ++, and +++) (yellow histogram, almost unamenable to triggering by H). Optimal fusion is obtained by metastable F stabilities in the middle of the range.

strongly destabilized and dependent on the presence of the compound for efficient membrane fusion (45). Based on our conformation-dependent MAb data, we now expand this conclusion and predict that due to the poor triggering stimulus of MeV H/CD46, AS-48 facilitated the generation of substantially destabilized F

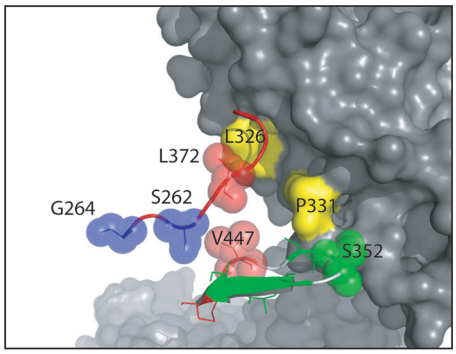

FIG 12 Fusion regulatory residues are located very close to the central pocket microdomain of the morbillivirus F trimer. Shown is a close-up view of the central pocket microdomain. Residues highlighted in red (V447T and L372A) and yellow (L326A and P331A) were identified in this study and shown to increase fusion by destabilizing the prefusion F trimer. Residues highlighted in blue (S262 [66] and G264 [65]) were reported to influence cell-cell fusion and viral pathogenicity.

trimers that were too labile to maintain the prefusion state in the absence of the drug. These F mutants henceforth required the presence of the compound to maintain an intracellular transport-competent prefusion conformation. This conclusion is corroborated by the data obtained with our structure-guided, destabilized MeV F-L457A V549A construct.

It is noteworthy that very similar observations were obtained regarding HIV Env resistance to the peptidic fusion inhibitor T20 (Fuzeon) (60). Although several pathways lead to HIV resistance to the peptide (61–63), T20-dependent HIV Env variants were isolated from treatment-experienced HIV patients (60). In this case, it was proposed that HIV Env was more prone to undergo premature refolding into the postfusion conformation; the presence of T20 delayed premature conformational changes and, in turn, Env inactivation. This T20 blockade was proposed to be only transient, and the spontaneous release of the peptide was considered to result in complete membrane fusion (60, 64).

Shirogane et al. (65) recently obtained mutant MeV particles with enhanced fusion activity that contained two types of genomes—one expressing a standard F trimer that could not be triggered by a modified H protein and the other an G264R F variant. It appeared that the enhanced fusion activity resulted from the formation of F heterotrimers, which compensated for the intrinsic fusion deficiencies of the two F proteins when assembled into homotrimers (65). While the authors directly assessed neither the conformational stability of these F complexes nor their physical interaction with H, they speculated that the inherent activation energy barrier of the heterotrimers reached the appropriate level to achieve productive H-dependent F triggering at the correct place and time (65). We note that the MeV F residue 264 is predicted to be located in very close proximity to the central pocket identified in our study (Fig. 12). These data thus support our conclusions and provide further evidence for a universal role of the central region of the morbillivirus F globular head domain in regulating the conformational stability of prefusion F.

We believe that the mechanism of F fusion triggering regulation illuminated by our model may affect the course of morbillivirus disease and viral pathogenesis. Watanabe and colleagues recently showed that mutations in the F ectodomain of wild-type MeV IC-B led to neurovirulence in immune-immature hamsters.

Interestingly, this phenotype correlated with enhanced F-mediated membrane fusion activity in SLAM- and nectin-4-negative cells (66). Some of the MeV F mutations described in this study are likewise located proximal to the central F pocket microdomain (Fig. 12), prompting us to speculate that the reportedly enhanced fusion activity resulted from destabilization of the mutated prefusion MeV F trimers. Also in the case of persistent CDV infection in the brain, we hypothesize that the strongly reduced fusion activity of CDV in astrocytes (48, 67, 68) may result, at least in part, from highly stable prefusion wild-type F trimers, which together with a suboptimal triggering stimulus (the cellular receptor involved is still unidentified) lead to poor fusion efficiency. These highly central nervous system (CNS)-specific conditions set the stage for predominant transmission of nucleocapsids from infected to neighboring cells in a noncytolytic manner, thus protecting the virus from immune recognition by bypassing massive syncytium formation and tissue destruction.

In conclusion, we demonstrate that the activation energy barrier of prefusion F trimers conformation together with the attachment protein-receptor combination define a "triggering range" that governs the initiation of the membrane fusion process. A central "pocket" microdomain in the globular F head contributes substantially to the regulation of the conformational stability of the prefusion complexes. The triggering range also defines the mechanism of viral escape from entry inhibitors and describes how the cellular environment can affect membrane fusion efficiency. Little is known about the exact link between membrane fusion activity in cell culture and morbillivirus pathogenesis. However, the disease spectrum—from massive cytolysis of lymphatic tissues accompanied by immunosuppression to noncytolytic persistent CNS infection—suggests that the triggering range may be an important determinant of the course of morbillivirus infection *in vivo*.

ACKNOWLEDGMENTS

We are grateful to Ulrike Holzgrabe and Georg Hiltensperger for providing the 3g fusion inhibitor. We also thank Marc Vandevelde for helpful comments on the manuscript.

This work was supported by the Swiss National Science Foundation reference no. 310030_132887 (to P.P.) and, in part, by Public Health Service grant AI083402 from the NIH/NIAID (to R.K.P.).

REFERENCES

1. **Chen SY, Anderson S, Kutty PK, Lugo F, McDonald M, Rota PA, Ortega-Sanchez IR, Komatsu K, Armstrong GL, Sunenshine R, Seward JF.** 2011. Health care-associated measles outbreak in the United States after an importation: challenges and economic impact. J. Infect. Dis. **203:** 1517–1525. http://dx.doi.org/10.1093/infdis/jir115.
2. **Sakai K, Nagata N, Ami Y, Seki F, Suzaki Y, Iwata-Yoshikawa N, Suzuki T, Fukushi S, Mizutani T, Yoshikawa T, Otsuki N, Kurane I, Komase K, Yamaguchi R, Hasegawa H, Saijo M, Takeda M, Morikawa S.** 2013. Lethal canine distemper virus outbreak in cynomolgus monkeys in Japan in 2008. J. Virol. **87:**1105–1114. http://dx.doi.org/10.1128/JVI.02419-12.
3. **Roelke-Parker ME, Munson L, Packer C, Kock R, Cleaveland S, Carpenter M, O'Brien SJ, Pospischil A, Hofmann-Lehmann R, Lutz H, Mwamengele GL, Mgasa MN, Machange GA, Summers BA, Appel MJ.** 1996. A canine distemper virus epidemic in Serengeti lions (Panthera leo). Nature **379:**441–445. http://dx.doi.org/10.1038/379441a0.
4. **Domingo M, Ferrer L, Pumarola M, Marco A, Plana J, Kennedy S, McAliskey M, Rima BK.** 1990. Morbillivirus in dolphins. Nature **348:**21. http://dx.doi.org/10.1038/348021a0.
5. **Lamb RA, Parks GD.** 2007. *Paramyxoviridae*: viruses and their replication, p 1449–1496. *In* Knipe D, Howley PM (ed), Fields virology5th ed, vol 1. Lippincott/Williams & Wilkins, Philadelphia, PA.
6. **Crennell S, Takimoto T, Portner A, Taylor G.** 2000. Crystal structure of the multifunctional paramyxovirus hemagglutinin-neuraminidase. Nat. Struct. Biol. **7:**1068–1074. http://dx.doi.org/10.1038/81002.
7. **Aguilar HC, Ataman ZA, Aspericueta V, Fang AQ, Stroud M, Negrete OA, Kammerer RA, Lee B.** 2009. A novel receptor-induced activation site in the Nipah virus attachment glycoprotein (G) involved in triggering the fusion glycoprotein (F). J. Biol. Chem. **284:**1628–1635. http://dx.doi.org/10.1074/jbc.M807469200.
8. **Chang A, Dutch RE.** 2012. Paramyxovirus fusion and entry: multiple paths to a common end. Viruses **4:**613–636. http://dx.doi.org/10.3390/v4040613.
9. **Plemper RK, Brindley MA, Iorio RM.** 2011. Structural and mechanistic studies of measles virus illuminate paramyxovirus entry. PLoS Pathog. **7:**e1002058. http://dx.doi.org/10.1371/journal.ppat.1002058.
10. **Hashiguchi T, Ose T, Kubota M, Maita N, Kamishikiryo J, Maenaka K, Yanagi Y.** 2011. Structure of the measles virus hemagglutinin bound to its cellular receptor SLAM. Nat. Struct. Mol. Biol. **18:**135–141. http://dx.doi.org/10.1038/nsmb.1969.
11. **Iorio RM, Melanson VR, Mahon PJ.** 2009. Glycoprotein interactions in paramyxovirus fusion. Future Virol. **4:**335–351. http://dx.doi.org/10.2217/fvl.09.17.
12. **Lamb RA, Jardetzky TS.** 2007. Structural basis of viral invasion: lessons from paramyxovirus F. Curr. Opin. Struct. Biol. **17:**427–436. http://dx.doi.org/10.1016/j.sbi.2007.08.016.
13. **Russell CJ, Jardetzky TS, Lamb RA.** 2001. Membrane fusion machines of paramyxoviruses: capture of intermediates of fusion. EMBO J. **20:**4024–4034. http://dx.doi.org/10.1093/emboj/20.15.4024.
14. **Brindley MA, Plemper RK.** 2010. Blue native PAGE and biomolecular complementation reveal a tetrameric or higher-order oligomer organization of the physiological measles virus attachment protein H. J. Virol. **84:**12174–12184. http://dx.doi.org/10.1128/JVI.01222-10.
15. **Colf LA, Juo ZS, Garcia KC.** 2007. Structure of the measles virus hemagglutinin. Nat. Struct. Mol. Biol. **14:**1227–1228. http://dx.doi.org/10.1038/nsmb1342.
16. **Hashiguchi T, Kajikawa M, Maita N, Takeda M, Kuroki K, Sasaki K, Kohda D, Yanagi Y, Maenaka K.** 2007. Crystal structure of measles virus hemagglutinin provides insight into effective vaccines. Proc. Natl. Acad. Sci. U. S. A. **104:**19535–19540. http://dx.doi.org/10.1073/pnas.0707830104.
17. **Takimoto T, Taylor GL, Crennell SJ, Scroggs RA, Portner A.** 2000. Crystallization of Newcastle disease virus hemagglutinin-neuraminidase glycoprotein. Virology **270:**208–214. http://dx.doi.org/10.1006/viro.2000.0263.
18. **Yuan P, Thompson TB, Wurzburg BA, Paterson RG, Lamb RA, Jardetzky TS.** 2005. Structural studies of the parainfluenza virus 5 hemagglutinin-neuraminidase tetramer in complex with its receptor, sialyllactose. Structure **13:**803–815. http://dx.doi.org/10.1016/j.str.2005.02.019.
19. **Bowden TA, Aricescu AR, Gilbert RJ, Grimes JM, Jones EY, Stuart DI.** 2008. Structural basis of Nipah and Hendra virus attachment to their cell-surface receptor ephrin-B2. Nat. Struct. Mol. Biol. **15:**567–572. http://dx.doi.org/10.1038/nsmb.1435.
20. **Xu K, Rajashankar KR, Chan YP, Himanen JP, Broder CC, Nikolov DB.** 2008. Host cell recognition by the henipaviruses: crystal structures of the Nipah G attachment glycoprotein and its complex with ephrin-B3. Proc. Natl. Acad. Sci. U. S. A. **105:**9953–9958. http://dx.doi.org/10.1073/pnas.0804797105.
21. **Bose S, Welch BD, Kors CA, Yuan P, Jardetzky TS, Lamb RA.** 2011. Structure and mutagenesis of the parainfluenza virus 5 hemagglutinin-neuraminidase stalk domain reveals a four-helix bundle and the role of the stalk in fusion promotion. J. Virol. **85:**12855–12866. http://dx.doi.org/10.1128/JVI.06350-11.
22. **Yuan P, Swanson KA, Leser GP, Paterson RG, Lamb RA, Jardetzky TS.** 2011. Structure of the Newcastle disease virus hemagglutinin-neuraminidase (HN) ectodomain reveals a four-helix bundle stalk. Proc. Natl. Acad. Sci. U. S. A. **108:**14920–14925. http://dx.doi.org/10.1073/pnas.1111691108.
23. **Deng R, Wang Z, Mirza AM, Iorio RM.** 1995. Localization of a domain on the paramyxovirus attachment protein required for the promotion of cellular fusion by its homologous fusion protein spike. Virology **209:**457–469. http://dx.doi.org/10.1006/viro.1995.1278.
24. **Tsurudome M, Kawano M, Yuasa T, Tabata N, Nishio M, Komada H, Ito Y.** 1995. Identification of regions on the hemagglutinin-neuraminidase protein of human parainfluenza virus type 2 important for promoting cell fusion. Virology **213:**190–203. http://dx.doi.org/10.1006/viro.1995.1559.

25. **Tanabayashi K, Compans RW.** 1996. Functional interaction of paramyxovirus glycoproteins: identification of a domain in Sendai virus HN which promotes cell fusion. J. Virol. **70:**6112–6118.
26. **Deng R, Mirza AM, Mahon PJ, Iorio RM.** 1997. Functional chimeric HN glycoproteins derived from Newcastle disease virus and human parainfluenza virus-3. Arch. Virol. Suppl. **13:**115–130.
27. **Wang Z, Iorio RM.** 1999. Amino acid substitutions in a conserved region in the stalk of the Newcastle disease virus HN glycoprotein spike impair its neuraminidase activity in the globular domain. J. Gen. Virol. **80:**749–753.
28. **Wang Z, Mirza AM, Li J, Mahon PJ, Iorio RM.** 2004. An oligosaccharide at the C-terminus of the F-specific domain in the stalk of the human parainfluenza virus 3 hemagglutinin-neuraminidase modulates fusion. Virus Res. **99:**177–185. http://dx.doi.org/10.1016/j.virusres.2003.11.010.
29. **Lee JK, Prussia A, Paal T, White LK, Snyder JP, Plemper RK.** 2008. Functional interaction between paramyxovirus fusion and attachment proteins. J. Biol. Chem. **283:**16561–16572. http://dx.doi.org/10.1074/jbc.M801018200.
30. **Paal T, Brindley MA, St. Clair C, Prussia A, Gaus D, Krumm SA, Snyder JP, Plemper RK.** 2009. Probing the spatial organization of measles virus fusion complexes. J. Virol. **83:**10480–10493. http://dx.doi.org/10.1128/JVI.01195-09.
31. **Brindley MA, Suter R, Schestak I, Kiss G, Wright ER, Plemper RK.** 2013. A stabilized headless measles virus attachment protein stalk efficiently triggers membrane fusion. J. Virol. **87:**11693–11703. http://dx.doi.org/10.1128/JVI.01945-13.
32. **Apte-Sengupta S, Negi S, Leonard VH, Oezguen N, Navaratnarajah CK, Braun W, Cattaneo R.** 2012. Base of the measles virus fusion trimer head receives the signal that triggers membrane fusion. J. Biol. Chem. **287:**33026–33035. http://dx.doi.org/10.1074/jbc.M112.373308.
33. **Tsurudome M, Ito M, Nishio M, Kawano M, Okamoto K, Kusagawa S, Komada H, Ito Y.** 1998. Identification of regions on the fusion protein of human parainfluenza virus type 2 which are required for haemagglutinin-neuraminidase proteins to promote cell fusion. J. Gen. Virol. **79:**279–289.
34. **Wild TF, Fayolle J, Beauverger P, Buckland R.** 1994. Measles virus fusion: role of the cysteine-rich region of the fusion glycoprotein. J. Virol. **68:**7546–7548.
35. **Tsurudome M, Ito M, Nishio M, Nakahashi M, Kawano M, Komada H, Nosaka T, Ito Y.** 2011. Identification of domains on the fusion (F) protein trimer that influence the hemagglutinin-neuraminidase specificity of the F protein in mediating cell-cell fusion. J. Virol. **85:**3153–3161. http://dx.doi.org/10.1128/JVI.01666-10.
36. **Yin HS, Wen X, Paterson RG, Lamb RA, Jardetzky TS.** 2006. Structure of the parainfluenza virus 5 F protein in its metastable, prefusion conformation. Nature **439:**38–44. http://dx.doi.org/10.1038/nature04322.
37. **Ader N, Brindley M, Avila M, Orvell C, Horvat B, Hiltensperger G, Schneider-Schaulies J, Vandevelde M, Zurbriggen A, Plemper RK, Plattet P.** 2013. Mechanism for active membrane fusion triggering by morbillivirus attachment protein. J. Virol. **87:**314–326. http://dx.doi.org/10.1128/JVI.01826-12.
38. **Brindley MA, Takeda M, Plattet P, Plemper RK.** 2012. Triggering the measles virus membrane fusion machinery. Proc. Natl. Acad. Sci. U. S. A. **109:**E3018–E3027. http://dx.doi.org/10.1073/pnas.1210925109.
39. **Ader N, Brindley MA, Avila M, Origgi FC, Langedijk JP, Orvell C, Vandevelde M, Zurbriggen A, Plemper RK, Plattet P.** 2012. Structural rearrangements of the central region of the morbillivirus attachment protein stalk domain trigger F protein refolding for membrane fusion. J. Biol. Chem. **287:**16324–16334. http://dx.doi.org/10.1074/jbc.M112.342493.
40. **Navaratnarajah CK, Negi S, Braun W, Cattaneo R.** 2012. Membrane fusion triggering: three modules with different structure and function in the upper half of the measles virus attachment protein stalk. J. Biol. Chem. **287:**38543–38551. http://dx.doi.org/10.1074/jbc.M112.410563.
41. **Plemper RK, Doyle J, Sun A, Prussia A, Cheng LT, Rota PA, Liotta DC, Snyder JP, Compans RW.** 2005. Design of a small-molecule entry inhibitor with activity against primary measles virus strains. Antimicrob. Agents Chemother. **49:**3755–3761. http://dx.doi.org/10.1128/AAC.49.9.3755-3761.2005.
42. **Sun A, Prussia A, Zhan W, Murray EE, Doyle J, Cheng LT, Yoon JJ, Radchenko EV, Palyulin VA, Compans RW, Liotta DC, Plemper RK, Snyder JP.** 2006. Nonpeptide inhibitors of measles virus entry. J. Med. Chem. **49:**5080–5092. http://dx.doi.org/10.1021/jm0602559.
43. **Plemper RK, Erlandson KJ, Lakdawala AS, Sun A, Prussia A, Boonsombat J, Aki-Sener E, Yalcin I, Yildiz I, Temiz-Arpaci O, Tekiner B, Liotta DC, Snyder JP, Compans RW.** 2004. A target site for template-based design of measles virus entry inhibitors. Proc. Natl. Acad. Sci. U. S. A. **101:**5628–5633. http://dx.doi.org/10.1073/pnas.0308520101.
44. **Singethan K, Hiltensperger G, Kendl S, Wohlfahrt J, Plattet P, Holzgrabe U, Schneider-Schaulies J.** 2010. *N*-(3-Cyanophenyl)-2-phenylacetamide, an effective inhibitor of morbillivirus-induced membrane fusion with low cytotoxicity. J. Gen. Virol. **91:**2762–2772. http://dx.doi.org/10.1099/vir.0.025650-0.
45. **Doyle J, Prussia A, White LK, Sun A, Liotta DC, Snyder JP, Compans RW, Plemper RK.** 2006. Two domains that control prefusion stability and transport competence of the measles virus fusion protein. J. Virol. **80:**1524–1536. http://dx.doi.org/10.1128/JVI.80.3.1524-1536.2006.
46. **Prussia AJ, Plemper RK, Snyder JP.** 2008. Measles virus entry inhibitors: a structural proposal for mechanism of action and the development of resistance. Biochemistry **47:**13573–13583. http://dx.doi.org/10.1021/bi801513p.
47. **Dayer AG, Jenny B, Sauvain MO, Potter G, Salmon P, Zgraggen E, Kanemitsu M, Gascon E, Sizonenko S, Trono D, Kiss JZ.** 2007. Expression of FGF-2 in neural progenitor cells enhances their potential for cellular brain repair in the rodent cortex. Brain **130:**2962–2976. http://dx.doi.org/10.1093/brain/awm200.
48. **Wyss-Fluehmann G, Zurbriggen A, Vandevelde M, Plattet P.** 2010. Canine distemper virus persistence in demyelinating encephalitis by swift intracellular cell-to-cell spread in astrocytes is controlled by the viral attachment protein. Acta Neuropathol. **119:**617–630. http://dx.doi.org/10.1007/s00401-010-0644-7.
49. **Plattet P, Langedijk JP, Zipperle L, Vandevelde M, Orvell C, Zurbriggen A.** 2009. Conserved leucine residue in the head region of morbillivirus fusion protein regulates the large conformational change during fusion activity. Biochemistry **48:**9112–9121. http://dx.doi.org/10.1021/bi9008566.
50. **Nussbaum O, Broder CC, Berger EA.** 1994. Fusogenic mechanisms of enveloped-virus glycoproteins analyzed by a novel recombinant vaccinia virus-based assay quantitating cell fusion-dependent reporter gene activation. J. Virol. **68:**5411–5422.
51. **Plattet P, Cherpillod P, Wiener D, Zipperle L, Vandevelde M, Wittek R, Zurbriggen A.** 2007. Signal peptide and helical bundle domains of virulent canine distemper virus fusion protein restrict fusogenicity. J. Virol. **81:**11413–11425. http://dx.doi.org/10.1128/JVI.01287-07.
52. **Sutter G, Ohlmann M, Erfle V.** 1995. Non-replicating vaccinia vector efficiently expresses bacteriophage T7 RNA polymerase. FEBS Lett. **371:**9–12. http://dx.doi.org/10.1016/0014-5793(95)00843-X.
53. **Orvell C, Sheshberadaran H, Norrby E.** 1985. Preparation and characterization of monoclonal antibodies directed against four structural components of canine distemper virus. J. Gen. Virol. **66:**443–456. http://dx.doi.org/10.1099/0022-1317-66-3-443.
54. **Zipperle L, Langedijk JP, Orvell C, Vandevelde M, Zurbriggen A, Plattet P.** 2010. Identification of key residues in virulent canine distemper virus hemagglutinin that control CD150/SLAM-binding activity. J. Virol. **84:**9618–9624. http://dx.doi.org/10.1128/JVI.01077-10.
55. **Langedijk JP, Janda J, Origgi FC, Orvell C, Vandevelde M, Zurbriggen A, Plattet P.** 2011. Canine distemper virus infects canine keratinocytes and immune cells by using overlapping and distinct regions located on one side of the attachment protein. J. Virol. **85:**11242–11254. http://dx.doi.org/10.1128/JVI.05340-11.
56. **Hasegawa K, Hu C, Nakamura T, Marks JD, Russell SJ, Peng KW.** 2007. Affinity thresholds for membrane fusion triggering by viral glycoproteins. J. Virol. **81:**13149–13157. http://dx.doi.org/10.1128/JVI.01415-07.
57. **Paterson RG, Russell CJ, Lamb RA.** 2000. Fusion protein of the paramyxovirus SV5: destabilizing and stabilizing mutants of fusion activation. Virology **270:**17–30. http://dx.doi.org/10.1006/viro.2000.0267.
58. **Russell CJ, Kantor KL, Jardetzky TS, Lamb RA.** 2003. A dual-functional paramyxovirus F protein regulatory switch segment: activation and membrane fusion. J. Cell Biol. **163:**363–374. http://dx.doi.org/10.1083/jcb.200305130.
59. **Waning DL, Russell CJ, Jardetzky TS, Lamb RA.** 2004. Activation of a paramyxovirus fusion protein is modulated by inside-out signaling from the cytoplasmic tail. Proc. Natl. Acad. Sci. U. S. A. **101:**9217–9222. http://dx.doi.org/10.1073/pnas.0403339101.
60. **Baldwin CE, Sanders RW, Deng Y, Jurriaans S, Lange JM, Lu M, Berkhout B.** 2004. Emergence of a drug-dependent human immunodeficiency virus type 1 variant during therapy with the T20 fusion inhibitor. J. Virol. **78:**12428–12437. http://dx.doi.org/10.1128/JVI.78.22.12428-12437.2004.
61. **Eggink D, Bontjer I, Langedijk JP, Berkhout B, Sanders RW.** 2011. Resistance of human immunodeficiency virus type 1 to a third-generation

fusion inhibitor requires multiple mutations in gp41 and is accompanied by a dramatic loss of gp41 function. J. Virol. **85:**10785–10797. http://dx.doi.org/10.1128/JVI.05331-11.
62. **Eggink D, Langedijk JP, Bonvin AM, Deng Y, Lu M, Berkhout B, Sanders RW.** 2009. Detailed mechanistic insights into HIV-1 sensitivity to three generations of fusion inhibitors. J. Biol. Chem. **284:**26941–26950. http://dx.doi.org/10.1074/jbc.M109.004416.
63. **Eggink D, Baldwin CE, Deng Y, Langedijk JP, Lu M, Sanders RW, Berkhout B.** 2008. Selection of T1249-resistant human immunodeficiency virus type 1 variants. J. Virol. **82:**6678–6688. http://dx.doi.org/10.1128/JVI.00352-08.
64. **Berkhout B, Eggink D, Sanders RW.** 2012. Is there a future for antiviral fusion inhibitors? Curr. Opin. Virol. **2:**50–59. http://dx.doi.org/10.1016/j.coviro.2012.01.002.
65. **Shirogane Y, Watanabe S, Yanagi Y.** 2012. Cooperation between different RNA virus genomes produces a new phenotype. Nat. Commun. **3:**1235. http://dx.doi.org/10.1038/ncomms2252.
66. **Watanabe S, Shirogane Y, Suzuki SO, Ikegame S, Koga R, Yanagi Y.** 2013. Mutant fusion proteins with enhanced fusion activity promote measles virus spread in human neuronal cells and brains of suckling hamsters. J. Virol. **87:**2648–2659. http://dx.doi.org/10.1128/JVI.02632-12.
67. **Vandevelde M, Zurbriggen A.** 2005. Demyelination in canine distemper virus infection: a review. Acta Neuropathol. **109:**56–68. http://dx.doi.org/10.1007/s00401-004-0958-4.
68. **Zurbriggen A, Graber HU, Wagner A, Vandevelde M.** 1995. Canine distemper virus persistence in the nervous system is associated with noncytolytic selective virus spread. J. Virol. **69:**1678–1686.